Estimation of ozone with total ozone portable spectroradiometer instruments. I. Theoretical model and error analysis

Lawrence E. Flynn, Gordon J. Labow, Robert A. Beach, Michael A. Rawlins, and David E. Flittner

Inexpensive devices to measure solar UV irradiance are available to monitor atmospheric ozone, for example, total ozone portable spectroradiometers (TOPS instruments). A procedure to convert these measurements into ozone estimates is examined. For well-characterized filters with 7-nm FWHM bandpasses, the method provides ozone values (from 304- and 310-nm channels) with less than 0.4% error attributable to inversion of the theoretical model. Analysis of sensitivity to model assumptions and parameters yields estimates of ±3% bias in total ozone results with dependence on total ozone and path length. Unmodeled effects of atmospheric constituents and instrument components can result in additional ±2% errors. © 1996 Optical Society of America

Key words: Ozone retrievals, surface UV.

1. Introduction

Ground-based measurements of UV radiation from Dobson and Brewer spectrophotometers have been used to estimate column ozone for over 60 years.[1] These instruments measure the direct or diffuse UV energy at the Earth's surface at multiple wavelengths with less than 1-nm band-passes. Column ozone (O_3) retrievals use four or more wavelengths to adjust for the effects of aerosols, sulfur dioxide (SO_2), and other wavelength-dependent factors. The use of measurements of the UV spectra from 290 nm to 350 nm (in steps of 0.5 nm with a bandpass of 0.9 nm) with a double monochromator to estimate O_3 was recently documented.[2]

In this paper we examine some of the problems associated with the estimation of ozone from measurements made by inexpensive, wideband, multiple-channel UV spectroradiometers. The slit-averaged-parameter models that work well with narrow-band instruments do not model adequately the channel responses of wider-band UV measuring devices. Channel responses are integrals of products of filter transmissivities, solar irradiance, and atmospheric attenuation. We approximate these integrals with independently measured quantities, summed over 1-Å bands. A multinomial model is constructed to fit the log of a ratio of responses from a pair of channels as a function of total column ozone and path length. The model is inverted to give total column ozone as a function of the channel ratios and the path lengths. Once an instrument is calibrated, a pair of measurements gives an estimate of total column ozone.

2. Description and Theory

The total ozone portable spectroradiometers (TOPS) family of instruments have been designed to make measurements of the direct solar irradiance in three channels, each of which responds to the flux in a region of the UV spectrum.[3] These measurements can be used to produce estimates of column ozone. The theory assumes that the measured intensity of filtered direct sunlight $I_{[\lambda]}$, for some interval about a wavelength λ, can be approximated by Beer's law:

$$I_{[\lambda]}(\Omega, s, P_0) \approx \bar{F}_\lambda \bar{T}_\lambda \bar{D}_\lambda \exp[-(\bar{\beta}_\lambda P_0 + \bar{\alpha}_\lambda \Omega) s], \quad (1)$$

L. E. Flynn is with the Software Corporation of America, 4601 Presidents Drive, Lanham, Maryland 20706. G. J. Labow and D. E. Flittner are with Hughes STX Corporation, 4400 Forbes Boulevard, Lanham, Maryland 20706. R. A. Beach and M. A. Rawlins were employed in 1994 and 1995, respectively, by the Summer Institute on Atmospheric and Hydrospheric Science at NASA Goddard Space Flight Center. R. A. Beach is now in graduate school at the California Institute of Technology, Pasadena, California 91103. M. A. Rawlins is at 102 Rolling Drive, Newark, Delaware 19713.

Received 2 January 1996; revised manuscript received 4 April 1996.

0003-6935/96/306076-08$10.00/0

where the overbar denotes weighted-average values over the interval of contributing wavelengths; α_λ is the ozone absorption coefficient in $(\text{atm cm})^{-1}$ and β_λ is the Rayleigh-scattering coefficient in atm^{-1}; T_λ is the filter transmissivity; F_λ is the solar irradiance at the top of the atmosphere; D_λ is attenuation by particulate scattering, SO_2, and other absorbers (all for an interval about a specific λ); P_0 is the surface pressure in atm; Ω is the column ozone in atm cm [Dobson units (DU) $\times 10^{-3}$]; and s is the secant of the solar zenith angle (SZA). The s values are used to approximate the relative path length through the atmosphere; $s = 1$ for SZA of 0°. An estimate of $\bar{F}_\lambda$ is obtained by the construction of a Langley plot,[3] although this is problematic even with narrow bandpass instruments.[4] If D_λ is a slowly varying function of λ, then ratios of measurements at two nearby UV wavelengths will be sensitive to changes in total column ozone, pressure, and path length, but insensitive to many other factors.

The simple relation in Eq. (1) is not accurate sufficiently to model the measured irradiances when a channel responds to an extended range of UV wavelengths, as is the case with the microcomputer-controlled TOPS (microTOPS) instruments. The relative contributions to a channel from different wavelengths vary with total ozone and path length. A single set of averaged parameters cannot model these variations accurately. A more complex model, which accounts for these changes, must be used. Figure 1 shows the transmissivity T_λ curves for the three filters (nominally centered at 298, 304, and 310 nm) used in microTOPS instrument #21 (MTOPS21). The 298- and 304-nm channels include UV-A blocking filters. The two other curves in each plot are discussed below.

A more realistic model of the filtered direct solar irradiance entering each channel is constructed. First, the irradiance in a 1-Å interval centered at each unit angstrom is modeled by

$$i_\lambda(\Omega, s, P_0) = F_\lambda T_\lambda \exp[-(\beta_\lambda P_0 A_1(s) + \alpha_\lambda \Omega A_2(s))], \quad (2)$$

where α_λ, β_λ, T_λ, F_λ, P_0, Ω, and s are as defined above for Eq. (1), and $A_1(s)$ and $A_2(s)$ give the relative path lengths through the atmosphere for Rayleigh scattering and ozone absorption, respectively. This model uses spherical shells to transform s into better estimates of the relative path lengths. Specifics for these two transformations and the accuracy of the estimates are discussed in Subsection 3.E. (The D_λ term has been neglected for this part of the analysis, but is also discussed in Subsection 3.C.)

Figure 2 shows the O_3 absorption coefficients α, the Rayleigh-scattering coefficients β, the SO_2 absorption coefficients γ, and the extraterrestrial solar irradiance F as functions of wavelength λ in the region of interest. The α values are computed assuming a temperature of 223 K.[5] The β values come from the work of Bates.[6] The γ values are taken from Ahmed and Kumar.[7] Their data were measured at room temperature every sixth of a nanometer from 280 to

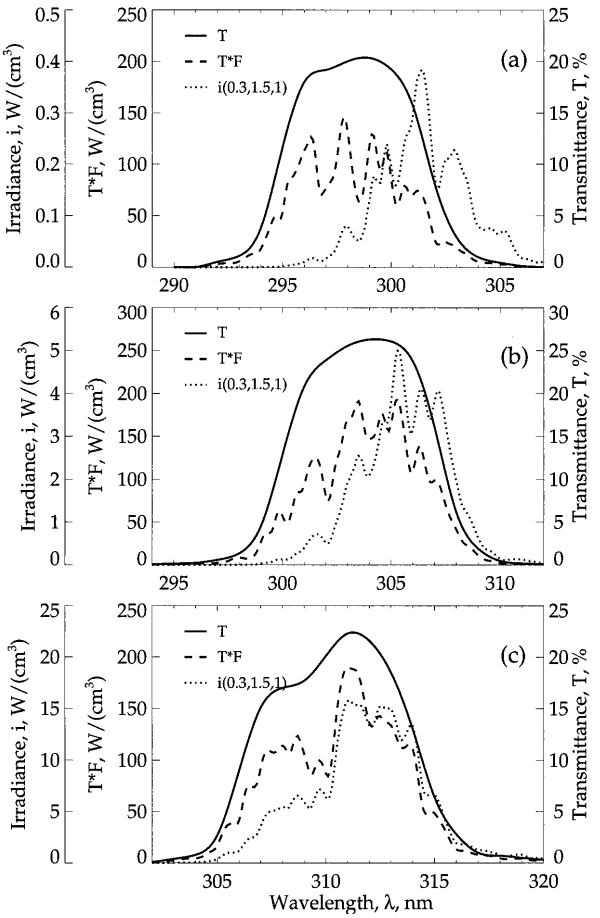

Fig. 1. (a) Filter-related information for the 298-nm channel. The solid curve is the transmittance T_λ in percent, and the scale is on the right. The dashed curve is the product of the transmittance and the extraterrestrial solar irradiance $T_\lambda F_\lambda$ in $\text{W/(cm}^3)$, and the scale is the near axis on the left. The dotted curve is the irradiance i_λ (0.3, 1.5, 1) in $\text{W/(cm}^3)$ (i.e., the modeled irradiances for $s = 1.5$, $\Omega = 0.3$ atm cm, and $P_0 = 1$ atm), and the scale is on the far left. (b) Filter-related information for the 304-nm channel. The labeling and axes are as described for Fig. 1(a). (c) Filter-related information for the 310-nm channel. Labeling and axes are as in Fig. 1(a).

320 nm. The extraterrestrial solar irradiances were interpolated to unit angstrom values from version 8 of the data measured by the Solar Stellar Irradiance Comparison Experiment on the Upper Atmosphere Research Satellite. The data were obtained with 2-Å resolution and better than 2% relative accuracy over the 290–320-nm interval.[8] Note that α decreases by an order of magnitude from 295 to 310 nm, and a typical value of Ω in Eq. (2) is 0.300 atm cm (300 DU).

The filtered extraterrestrial solar irradiance $T_\lambda F_\lambda$ as a function of λ [i.e., the product of the first two terms on the right-hand side of Eq. (2)] is given by the dashed curves in Fig. 1. The irradiances $i_\lambda(0.3, 1.5, 1)$ [i.e., $i_\lambda(\Omega, s, P_0)$ of Eq. (2) with $s = 1.5$, $\Omega = 0.3$ atm cm (300 DU), and $P_0 = 1$ atm] are given by the dotted curves in Fig. 1. Note that the relative contributions for each channel shift to longer wavelengths because

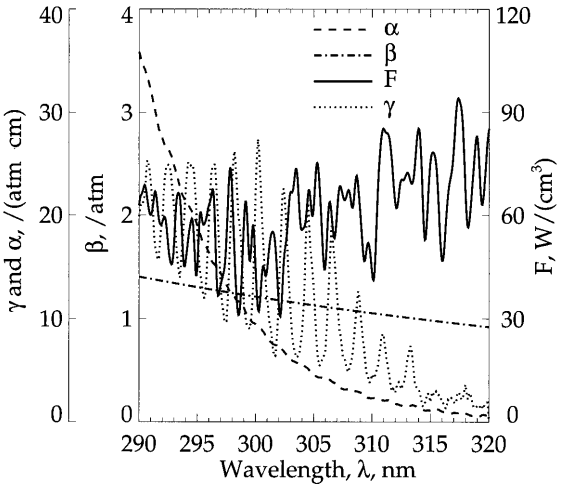

Fig. 2. Important physical data for the 290–320-nm range. The solid curve is the extraterrestrial solar irradiance F_λ in W/(cm^3), and the scale is on the right. The dash–dot curve is the Rayleigh-scattering coefficient β_λ in atm^{-1}, and the scale is on the near axis on the left. The dotted curve is the SO_2 absorption cross section γ_λ, and the dashed curve is the O_3 absorption cross section α_λ, both in atm cm and sharing the scale on the far-left axis.

of the decrease in α_λ with wavelength. Significant contributions to the 298-nm channel are present above 304 nm, even though the transmissivity in that region is below 1%. The scale for i_λ relative to F is 1:500 for the 298-nm channel, 1:50 for the 304-nm channel, and 1:10 for the 310-nm channel. The microTOPS instruments use different gains to amplify the signals in the different channels appropriately.

The total irradiance for each channel is given by an integral of i_λ, which we approximate by

$$I_{[\Lambda]} = \sum_{m_\Lambda \le \lambda \le M_\Lambda} i_\lambda, \tag{3}$$

where Λ = 298-nm, 304-nm, or 310-nm channel; m_Λ and M_Λ are lower and upper limits on the contributing wavelengths; and λ is incremented in steps of 1 Å.

The actual counts measured by an individual microTOPS channel are scaled by the photodiode efficiencies and amplifier gains of that channel. In addition there are other atmospheric absorbers and particulate scatterers. If relative channel efficiencies and gains are constant over time, and if effects of particulate scatters and other atmospheric absorbers are relatively wavelength independent, then a ratio of model $I_{[\Lambda]}$ values for two channels is proportional to the corresponding ratio of measured microTOPS channel counts. We define the calibration constant $\Re$, which converts a model ratio into an observed instrument ratio, by

$$\Re I_{[304]}/I_{[310]} = N_{[304]}/N_{[310]}, \tag{4}$$

where $N_{[\Lambda]}$ is the count measured by the instrument for the Λ channel. Then, given a measured ratio, with pressure and SZA information, one inverts the calibrated model to determine the column ozone. (Practical experiences with calibration and inversion of this model are presented in a companion paper in this issue.[9])

The model was used to estimate the ratio $R(\Omega, s) = I_{[304]}/I_{[310]}$ for a grid of s and Ω values with $P_0 = 1$, s = 1.0 to 3.0 in steps of 0.1, and Ω = 0.200 to 0.500 in steps of 0.010 atm cm. Simple multinomials in Ω and s were fit to the surface, log (R) versus (Ω, s). One of the form,

$$\log[R(\Omega, s)] \approx C_0 + C_1 s + C_2\Omega + C_3 s^2 + C_4\Omega^2 + C_5\Omega s + C_6\Omega^2 s + C_7\Omega s^2 + C_8 s^3, \tag{5}$$

was found to fit $\log[R(\Omega, s)]$ with less than 0.004 absolute error. The percent errors in the estimation of ozone with this nine-term fit, instead of the full model, are shown in Fig. 3(a). A nice feature of this multinomial form is that it is only quadratic in Ω and may be inverted easily to solve for Ω given estimates of $R(\Omega, s)$ and s. Only one of the roots produces a physically reasonable ozone estimate. The values of C_i for MTOPS21 with $P_0 = 1$ are given in Table 1, column 2. Other columns of Table 1 and contour plots in Fig. 3 are discussed in Section 3.

3. Errors and Adjustments

One can find the effects of changes in various parameters and components on the modeled ratio to estimate (and correct) the errors in the derived ozone. Several such analyses are presented in this section. The results of the analyses are presented in Figs. 3(a)–(f) as contour plots showing the errors as functions of s and column ozone and in Table 1 as values of d_{pi}, d_{si}, and d_{ti} to make linear corrections to the C_i values for known conditions.

A. Calibration Constant

The instrument to model ratio $\Re$ can be determined by calibration with a previously calibrated instrument (with identical filters) or by calibration with ozone estimates from another source. The latter procedure is examined in Ref. 9. Although this paper does not cover the practical determination of the calibration constant $\Re$, the sensitivity of the ozone estimates to errors in this constant is determined easily. The effects of a 1% error in $\Re$ on the derived ozone values are given in Fig. 3(b). These values also give the reciprocal of the sensitivity of the instrument pair ratio, that is, the percent ozone changes derived from 1% changes in the measured ratios.

B. Atmospheric Pressure

Day-to-day variations in atmospheric pressure of 1% or 2% are common, and even larger changes may accompany particularly strong weather fronts. These variations produce changes in the measurements and should be accounted for in the model. The effects are not large and can be approximated if one makes linear changes to the C_i values. The changes in the C_i's for a 5% change in P_0 from P_0 = 1 atm are found by fitting Eq. (5) to the model with P_0 = 1.05 atm and are given by the d_{pi}'s in Table 1,

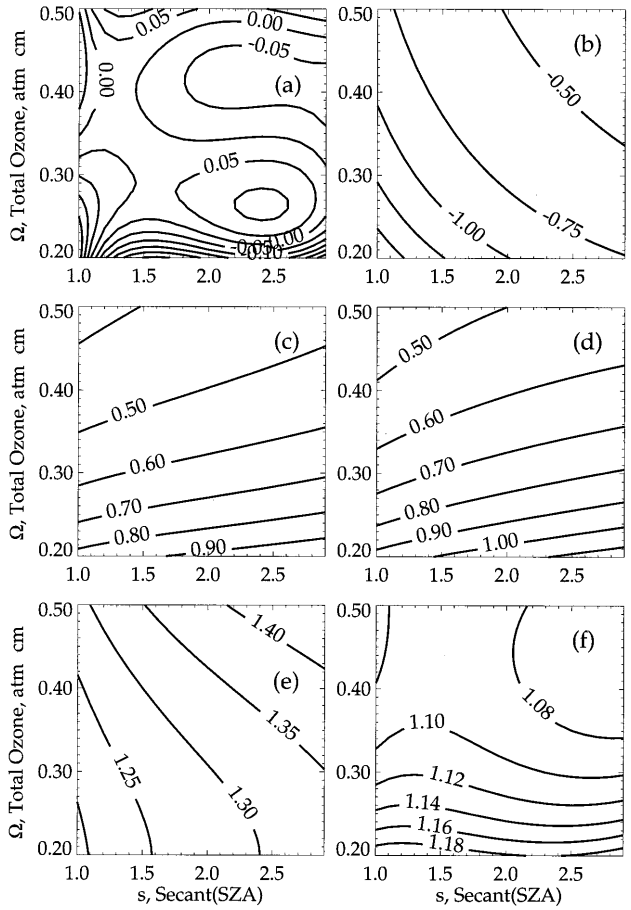

Fig. 3. All six contour plots show the percent error in column ozone estimates versus s and Ω. (a) Errors from the use of 9-term multinominal to approximate model results. (b) Errors from a −1% error in ℜ. (c) Errors from a −5% error in P_0. (d) Errors from 0.001 atm cm of SO_2. (e) Errors from −10 K error in atmospheric temperature. (f) Errors from a −1% error in s.

column 3. If pressure data are available, then the model C_i's (Table 1, column 2) can be adjusted by

$$C_i(P) = C_i + (P - P_0)d_{pi}/0.05, \qquad (6)$$

where P is the actual pressure. The adjustments to the model ratios for a ±5% range of pressure changes,

Table 1. Parameters in a Nine-Term Fit to Model and Linear Corrections for Pressure, SO_2, and Temperature Errors

i	Model C_i	0.05 atm d_{pi}	1-DU SO_2 d_{si}	10 K d_{ti}
0	0.06067	−0.00018	−0.00116	−0.00138
1	−0.26710	−0.00517	−0.00412	0.00102
2	−0.37100	0.00014	0.00511	0.00608
3	0.04916	0.00015	0.00046	−0.00031
4	−0.08957	−0.00018	−0.00497	−0.01031
5	−3.03792	0.00167	−0.00505	−0.04155
6	0.82468	−0.00116	0.00368	0.01415
7	0.18372	0.00002	0.00120	0.00293
8	−0.00810	−0.00001	0.00004	0.00000

with Eq. (6), match the computed changes in $R(\Omega, s)$ within 2% *of the changes*.

Figure 3(c) shows the percent error in the derived ozone resulting from an uncorrected 5% error in the pressure (real pressure for the measurements 5% larger than used in the model) as a function of the real ozone and secant of the SZA values. Notice that this 5% error produces an ozone error of about 0.002 atm cm. If an instrument is to be operated at a high-altitude location, then a new set of C_i values should be computed for the nominal pressure of the site.

C. Other Scatterers and Absorbers

One of the factors hidden in the neglected D_λ term is absorption by atmospheric SO_2. Background levels of SO_2 are usually less than 0.001 atm cm, although urban and industrial areas with polluted boundary layers may have 0.005 atm cm or larger values.[10] Volcanic plumes may produce elevated SO_2 amounts of 0.030 atm cm or more moving over 10^5 km^2 regions and lasting for several days.[11] The model ratios are recomputed, including the attenuation attributable to 0.001 atm cm of SO_2 with the γ_λ values of Fig. 1. An additional term of 0.001 γ_λ s is added to the exponent in Eq. (2). The γ_λ values do have a large wavelength dependence.

The errors in the derived ozone if 0.001 atm cm of SO_2 is present and unaccounted for appear in Fig. 3(d). This plot is much flatter if the errors are expressed as an absolute ozone change instead of percent—0.001 atm cm of SO_2 produces about 0.002 atm cm of derived ozone error. If levels of SO_2 are known, then the d_{si} values in Table 1, column 4, can be used to make first-order adjustments to the C_i's in column 2 prior to an estimation of the total column ozone. The adjustment for as much as 0.005 atm cm of SO_2, with the d_{si} data, fit the computed changes in $R(\Omega, s)$ within 5% *of the changes*. Given the uncertainty in the knowledge of the SO_2 cross sections, one expects errors of the order of 0.5 atm cm of O_3 per atm cm of SO_2 even after making these corrections.[12]

Aerosols, dust, mists, and other scatterers and absorbers (excluding SO_2) lumped into the D_λ term affect the accuracy of the derived ozone estimates. This attenuation reduces the solar irradiance at the Earth's surface by as much as a factor of 10, even in cloud-free skies. Conservatively high estimates of the wavelength dependence of the optical depth of such components give 1% differences (up *or* down) in the optical depth between the 304-nm and 310-nm channels.[13] This effect could be much larger in the presence of a monodisperse aerosol.

The ozone error from such dependence is now a function of the optical depth of these various absorbers and scatterers. Multiplying the right-hand side of Eq. (2) by a D_λ of the form given in Eq. (7), we obtain a model that takes such scattering into account.

$$D_\lambda = \exp\{-\tau[1 + 0.01(\lambda - 300)/6]s\}, \qquad (7)$$

where τ is the optical depth of the haze at 300 nm, λ is the wavelength in nanometers, and s is the secant of the SZA. The constants in Eq. (7) have been selected so that there is a 1% increase in the optical depth per 6-nm change in λ. The model ratios were computed for $\tau = 1$ (resulting in about one seventh of the unattenuated signal for $s = 2$). The new $R(\Omega, s)$ values are very similar to those produced by the multiplication of the old $R(\Omega, s)$ values by $(1 + 0.01\ s)$. This is not surprising because the main effect on $R(\Omega, s)$ of the wavelength-dependent optical depth, as approximated here, for a fixed s should appear as an interchannel calibration offset of approximately $\tau \times s\%$. Thus multiplying the errors presented by Fig. 3(b) by s will provide estimates of the errors from this source. They range from 0.8% to 2.2% (0.003 to 0.006 atm cm) for the D_λ of Eq. (7).

Although a reduction of a factor of 7 in the individual UV channel signals should be recognized easily with frequent use of a stable instrument, determination of the wavelength dependence of the attenuation to correct the ozone estimates requires external information. Practical problems caused by aerosols for real measurements are observed in Ref. 9.

The direct sun model of Eq. (2) assumes that forward-scattering contributions will be very small. To estimate the contribution attributable to diffuse light scattered into the field of view, theoretical simulations of the diffuse light field were performed for a model atmosphere. The theoretical model includes all orders of scattering, a Lambert reflecting surface, molecular anisotropy, polarization, and spherical attenuation of the direct solar beam.[14,15] In these simulations the aerosol vertical profile was taken from Elterman,[16] and the size distribution was modeled with a constant number density for the 0.005–0.1 -μm radii range and a Junge parameter of 3 for the radii between 0.1 and 7.0 μm, with a refractive index of $1.55 + i0.0$. The aerosol optical depth was set to 0.2 at 298 nm and was allowed to vary at the other wavelengths according to Mie calculations, and the total column ozone was set at 0.325 atm cm. For a surface albedo of 0.1, $s = 3$ (SZA = 71°), and 3° field of view, the ratios of diffuse-to-direct flux are 11.8, 1.26, and 1.1% for the 298-nm, 304-nm, and 310-nm channels, respectively. At 0° SZA the ratios decrease for all channels to approximately 0.32%. The weak wavelength dependence of the diffuse flux contributions for the 304-nm and 310-nm channels causes the direct flux model ratios $R(\Omega, s)$ to differ from the detailed simulation ratios by less than 0.2% for $s \leq 3$ and a field of view $\leq 3°$. The 298–304-nm ratios can differ by 10% or more in the same circumstances.

D. Temperature Dependence of Ozone Cross Sections

In constructing the model, we computed the α_λ values in Eq. (2) at a temperature of 223 K. This temperature is representative of the average column temperature weighted by the ozone concentration. The actual temperatures vary with height, latitude, and season. Channel 4 temperature data from the Microwave Sounding Unit (MSU) of the National Oceanic and Atmospheric Administration operational satellites provide a weighted average of the temperatures of the lower stratosphere.[17] Because this region of the atmosphere is also the location of the peak ozone concentrations, changes in the MSU temperatures quantify the temperature variations for α calculations. Monthly average MSU temperatures for $10° \times 30°$ latitude by longitude bins centered on 40°N are almost always between 205 K and 215 K over the 1980–1990 period (and usually between 200 K and 230 K for all $10° \times 30°$ bins from 60°S to 60°N).

The model ratios were recomputed with α_λ calculated for a 10 K warmer temperature. The estimated ozone errors attributable to this change are shown in Fig. 3(e). If more accurate temperature data are available, then the d_{ti} values in Table 1, column 5, can be used to correct the model C_i's before ozone values are derived. That is,

$$C_i(T) = C_i + (T - 223)d_{ti}/10, \tag{8}$$

where T is the ozone-weighted mean column temperature in kelvin. The adjustment for ± 10 K about 223 K, with the d_{ti}'s, fit the computed changes in $R(\Omega, s)$ within 10% *of the changes*.

E. Path-Length Estimation

The path-length calculations use the equation of time and other formulas[18] to determine the SZA, and they depend on accurate knowledge of the time and latitude and longitude. A known SZA error is corrected directly. The most common errors are in the times of measurements. A 1-min error in time of measurement or a 15-arcmin error in either latitude or longitude results in at most a 0.75% error at $s = 2$ and at most a 1.5% error at $s = 3$. At 45°N, a 15-arcmin error in longitude is equivalent to a 20-km error in east-west location. The sign of the s error switches at local solar noon for time or longitude errors. Small changes in s produce almost identical changes in the relative path-length estimates $A_1(s)$ and $A_2(s)$. The results of a 1% error in s (real s is 1% larger than used to derive ozone) are shown in Fig. 3(f). Errors in time and location transform into errors in s in a complicated manner, but, in general, the errors are smallest at local solar noon.

The $A_1(s)$ and $A_2(s)$ functions in Eq. (2) are designed to account for the spherical nature of the atmosphere and the vertical distribution of ozone. They use 11 spherical shells defined by the standard Umkehr layers. Each layer is about 5-km thick and contains approximately one half of the atmosphere above its lower boundary. The ozone distribution is given by a standard 0.375-atm cm mid-latitude profile.[19] The atmosphere amounts (or ozone amounts) within the shells times the effective geometric path at the center of the shells are summed,[20] and the total is divided by the total atmosphere (or column ozone). For Rayleigh scattering, the effective path lengths are within 1% of s and are very accurate. For ozone absorption, they are within 2.5% of s, for s less than

3, and their accuracy depends on the real ozone distribution.

The ozone profile used here was selected because it provides $A_1(s)$ values that are in the middle of those obtained for 22 other standard profiles.[19] These profiles have total ozone amounts from 0.125 to 0.575 atm cm and are representative of ozone distributions from low, mid, and high latitudes. The absolute differences in the shell estimates for the selected ozone profile and this larger set are less than 0.5% up to $s = 3$.

F. Extraterrestrial Solar Irradiance

Variations in F_λ for this spectral region over the 11-year solar cycle and 27-day solar rotation are small. By using scale factors and Mg II index information,[21] one finds that the changes in F_λ from solar minimum to solar maximum for wavelengths in the 295-nm to 320-nm region range from 0.0% to 0.5%. These variations are not monotone with wavelength and result in even less error than a 0.5% change in the calibration constant $\Re$. Relative changes in extraterrestrial insolation due to Earth orbit eccentricity are wavelength independent and cause no errors.

G. Instrument Responses

The instruments have two spectral response properties that lead to errors in the derived ozone. The first is the dependence of the responsivity of the photodiodes on wavelength. This acts like a wavelength-dependent transmissivity and can be included in the T_λ term if known. Only within-channel variations are important as interchannel differences are included in the calibration constant $\Re$. Over the 30-nm ranges of interest, the MicroTOPS photodiodes are thought to have less than 5% variation in their response. If always present and approximately linear in λ, then most of the errors are countered by a change in $\Re$, and the derived ozone errors are less than 0.1%.

The second complication is deviations of the responsivity with instrument-operating temperatures. Differences in this deviation that are a function of wavelength are important. The MicroTOPS instruments use gallium phosphide photodiodes that have up to 0.5%/6 nm difference in response for 10 K change in instrument temperature at approximately 300 K. This response change is modeled when one multiplies the T_λ by $[1 - 0.005\ (\lambda - 300)/6]$ and recomputes $R(\Omega, s)$. The new $R(\Omega, s)$ are very similar to those produced when one multiplies the old $R(\Omega, s)$ by 1.005. This is not surprising because the main effect of the wavelength-dependent optical depth on $R(\Omega, s)$ appears as an interchannel calibration offset. The result of an uncorrected 0.5% increase in the measurements, relative to the calibrated model, on the derived ozone is estimated when one multiplies the data in Fig. 3(b) by one half. The abilities of users to control the temperatures of instruments at time of use vary.

H. Accuracy and Stability of Filter Transmissivity

Accurate knowledge of filter transmissivities, especially in the upper wings, is important for accurate modeling. The T_λ values used here are those for the filters in MTOPS21 as measured by Barr Associates, Inc., Westford, Mass. To test the sensitivity of the models, we altered the T_λ values for the 304- and 310-nm channels in three different ways. The first test involves increasing the T_λ by 0.5% (absolute) over various 1-nm ranges within 6 nm of the channel center. As expected, the modeled $R(\Omega, s)$ values are most sensitive to changes in the upper range of the 304-nm channel. The largest changes in the modeled $R(\Omega, s)$ values for 304-nm-channel 0.5% increases are 0% to 2% ([308, 309] interval) and 0.3% to 3.5% ([309, 310] interval). For the 310-nm channel, the largest changes are 0% to -1% ([315, 316] interval).

The second test involves increasing the T_λ by 10% (relative) over various 1-nm ranges. The largest changes in the modeled $R(\Omega, s)$ values are 1% to 3% for changes in the 304-nm channel and 0% to -2% in the 310-nm channel. Because the T_λ term is multiplied by the F_λ term, this test also quantifies the errors that are produced by 10% relative errors over 1-nm ranges in the extraterrestrial irradiance estimates.

The third test models a 0.5-Å error in wavelength registration during calibration of the filter bandpasses. When the T_λ data are shifted to the right by 0.5 Å, the new $R(\Omega, s)$ values are 5% to 8% higher. In all three cases, the changes in $R(\Omega, s)$ values for the tested 304-nm-channel perturbations are monotone increasing as functions of Ω and s. If the real filters differed in any of these ways, then the calibration constant $\Re$ adjusts for at least the minimum change. The final effects on the ozone estimates depend on the percent differences in $R(\Omega, s)$ between the time of calibration and the times of measurements. The effects of these differences on the derived ozone are estimated from Fig. 3(b).

Questions about the stability of filters pose a serious and unresolved issue. Obviously if the filters' bandpasses change over time, then the model coefficients must be recalculated. Changes in filter characteristics would produce a variety of errors in the ozone estimates. These errors can be detected by periodic calibration either through direct measurement of known sources or comparisons against stable ozone monitoring devices. Such monitoring is necessary to guarantee the quality of long-term time series of ozone data from this type of instrument.

The analysis herein also has not addressed two other issues. The first issue concerns the presence of stray light and leakage in the filters. The UV-A blockers on the 304-nm channel and the reduced responsivity of the gallium phosphide photodiodes in the visible and infrared part of the spectrum act as compensating factors for this problem. The second issue concerns the linearity of the instrument responses over the wide range of signals encountered.

Table 2. Summary of Error Sources, Sizes, and Effects

Error Source	Size	Sensitivity or Error Range	Average Absolute (%)	Bias (%)	Comments
Nine-term model	1	−0.3–0.2%	0.1	±0.1	Dependence on s and O_3
$\Re$	1%	0.3–1.5	1	±1	Dependence on s and O_3
Pressure	2%	0.1–0.2	0.2	0	Some seasonal variations
SO_2	2 DU[a]	0.5–1.0% DU^{-1}	1	+1	Occasional extreme events
Aerosols	1 OD[b]	0.3–1.5% OD^{-1}	1	±1	Identify presence with single channels
Atmospheric temperature	5 K	0.1–0.2% K^{-1}	0.3	0	Seasonal bias, correct with external data
s	0.5%	0–1	0.2	0	Effort provides accuracy, bias in some cases
Sphericity		0–1%	0.1	−0.1	Important for $s > 2$
F_λ	0.5%	0.0–0.2	0.1	0	Only relative accuracy
Instrument temperature	10 K	0.0–0.1% K^{-1}	0.5	0	Should be controlled
T_λ	10% rel. 0.5% abs. 0.5 Å	−0.2–0.3 0–7 0–6% $Å^{-1}$	2	±2	Dependence on s and O_3

[a]1 DU = 0.001 atm cm.
[b]OD is optical depth.

We do not have enough information to address these issues, but problems observed with the 298-nm channel in Ref. 9 do raise concerns.

4. Summary and Conclusions

The goal of this research was to provide a step-by-step method with quantifiable errors to derive ozone estimates from surface UV measurements obtained with inexpensive, wide bandpass filters. Once determined, the C_i, d_{pi}, d_{si}, and d_{ti} data of Table 1, together with the function in Eq. (5), provide the basis for deriving estimates of the ozone from instrument measurements with a single calibration constant $\Re$. Table 2 classifies and summarizes the errors studied for the model presented in this paper. The first column designates the sources of the errors; the second gives physically realistic sizes for the errors; the third gives the sensitivities of the ozone estimates to the errors; the fourth and fifth provide estimates of the average absolute error and bias produced in the ozone estimates, respectively; and the sixth presents some comments on the behavior of the errors.

The main sources of bias in the derived ozone estimates (and estimates of the biases) are errors in filter or solar data (2%), uncertainty in the estimation of the calibration constant $\Re$ (1%), the presence of $S0_2$ (1%), the presence of aerosols and other absorbers and scatterers (1%), and changes in the atmospheric column temperatures (0.5%). Most of the other sources of error can be minimized by careful operation of the instruments, corrected with auxiliary information, or they are likely to be random and average out over multiple measurements during a day.

With the analysis outlined here we use only a single pair of measurements to estimate ozone. If other well-behaved UV channel measurements are available, one can retrieve jointly additional quantities, for example, SO_2 or the wavelength dependence of aerosol optical depth, as are obtained with five channels for the Brewer instruments.[22]

The authors acknowledge the assistance of frequent discussions with P. K. Bhartia, E. Celarier, J. Herman, E. Hilsenrath, A. Krueger, R. McPeters, and F. Mims. This study was supported by NASA contract NAS5-32376 and the University of Maryland, College Park/NASA/GSFC Summer Institute on Atmospheric and Hydrospheric Science 1994–1995.

References

1. World Meteorological Organisation, *Scientific Assessment of Ozone Depletion: 1994, Global Ozone Research and Monitoring Project*, Rep. No. 37 (World Meteorological Organisation, Geneva, 1995), and references therein.
2. M. Huber, M. Blumthaler, and W. Armbach, "Total atmospheric ozone determined from spectral measurements of direct solar irradiance," *Geophys. Res. Lett.* **22**(1), 53–56 (1995).
3. F. M. Mims, "How to measure the ozone layer," Sci. Probe **2,** 45–51 (1992).
4. J. A. Reagan, L. W. Thomason, B. M. Herman, and J. M. Palmer, "Assessment of atmospheric limitations on the determination of solar spectral constant from ground-based spectroradiometer measurements," IEEE Trans. Geosci. and Remote Sensing **24**(2), 258–266 (1986).
5. A. M. Bass and R. J. Paur, "The ultraviolet cross-sections of ozone. I. The measurements," *Atmospheric Ozone*, C. S. Zerefos and A. Ghazi, eds. (Reidel, Norwell, Mass., 1984) pp. 611–617.
6. D. R. Bates, "Rayleigh scattering by air," Planet. Space Sci. **32,** 785–790 (1984).
7. S. M. Ahmed and V. Kumar, "Quantitative photoabsorption and fluorescence spectroscopy of SO_2 at 188–231 and 278.7–320 nm," J. Quant. Spectrosc. Radiat. Transfer **47,** 359–373 (1992).
8. T. N. Woods, D. K. Prinz, G. J. Rottman, J. London, P. C. Crane, R. P. Cebula, E. Hilsenrath, G. E. Brueckner, M. D. Andrews, O. R. White, M. E. VanHoosier, L. E. Floyd, L. C. Herring, D. G. Knapp, C. K. Pankratz, and P. A. Reiser, "Validation of the UARS solar ultraviolet irradiances: compar-

ison with the ATLAS 1 and 2 measurements," J. Geophys. Res. **101,** 9541–9570 (1996).
9. G. J. Labow, L. E. Flynn, M. A. Rawlins, R. A. Beach, C. A. Simmons, and C. M. Schubert, "Estimation of ozone with total ozone portable spectroradiometer instruments. II. Practical operation and comparisons," Appl. Opt. **35,** 6084–6089 (1996).
10. D. De Muer and H. De Backer, "Revision of 20 years of Dobson total ozone data at Uccle (Belgium): fictitious Dobson total ozone trends induced by sulfur dioxide trends," J. Geophys. Res. **97**(D5), 5921–5937 (1992).
11. A. J. Krueger, L. S. Walter, P. K. Bhartia, C. C. Schnetzler, N. A. Krotkov, I. Sprod, and G. J. S. Bluth, "Volcanic sulfur dioxide measurements from the total ozone mapping spectrometer instruments," J. Geophys. Res. **100,** 14057–14076 (1995).
12. Compare results of Ahmed and Kumar[7] with those of T. J. McGee and J. Burris, Jr., "SO_2 absorption cross sections in the near UV," J. Quant. Spectrosc. Radiat. Transfer **37,** 165–182 (1987).
13. Extrapolation of theoretical calculations for four polydispersions in Fig. 5 of J. V. Dave, "Effect of aerosols on the estimation of total ozone in an atmospheric column from the measurements of its ultraviolet radiance," J. Atmos. Sci. **35,** 899–911 (1978).
14. B. M. Herman and S. B. Browning, "A numerical solution to the equation of radiative transfer," J. Atmos. Sci. **22,** 559–566 (1965).
15. B. M. Herman, S. B. Browning, and J. A. Reagan, "An analytic study of the solar aureole," presented at the International Radiation Symposium, Ft. Collins, Colo., August 11–16, 1980.
16. L. Elterman, "UV, visible and IR attenuation for altitudes to 50 km," AFCRL-68-1053 (U.S. Air Force Research Laboratory, Bedford, Mass., 1968).
17. R. W. Spencer and J. R. Christy, "Precision lower stratospheric temperature monitoring with the MSU: technique, validation and results 1979–1991," J. Clim. **6,** 1194–1204 (1993).
18. For example, see equations on p. C24 in *The Astronomical Almanac, for the Year 1986* (Nautical Almanac Office, U.S. Government Printing Office, Washington, D.C., 1985).
19. See Appendix D of R. D. McPeters, A. J. Krueger, P. K. Bhartia, J. R. Herman, A. Oaks, Z. Ahmad, R. P. Cebula, B. M. Schlesinger, T. Swissler, S. L. Taylor, O. Torres, and C. G. Wellemeyer, *Nimbus-7 Total Ozone Mapping Spectrometer* (*TOMS*) *Data Products User's Guide*, NASA Ref. Pub. 1323 (NASA, Washington, D.C., 1993).
20. See Appendix B of A. Dahlback and K. Stamnes, "A new spherical model for computing the radiation field available for photolysis and heating at twilight," Planet. Space Sci. **5,** 671–683 (1991).
21. M. T. DeLand and R. P. Cebula, "The composite Mg II solar activity index for solar cycles 21 and 22," J. Geophys. Res. **98,** 12809–12823 (1993).
22. W. J. F. Evans, H. Fast, A. J. Forester, G. S. Henderson, J. B. Kerr, R. K. R. Vupputuri, and D. I. Wardle, *Stratospheric Ozone Science in Canada: An Agenda for Research and Monitoring*, Internal Rep. ARD 87–3 (Atmospheric Environment Service, Downsview, Ontario, Canada, 1987).